

# Mechanism of exotic density-wave and beyond-Migdal unconventional superconductivity in kagome metal $AV_3Sb_5$ ( $A=K, Rb, Cs$ )

Rina Tazai, Youichi Yamakawa, Seiichiro Onari, and Hiroshi Kontani  
*Department of Physics, Nagoya University, Furo-cho, Nagoya 464-8602, Japan.*  
 (Dated: July 13, 2021)

Exotic quantum phase transitions in metals, such as the nematic and smectic states, were discovered one after another and found to be universal now. The emergence of unconventional density-wave order in frustrated kagome metal  $AV_3Sb_5$  and its interplay with exotic superconductivity attract increasing attention. We reveal that the smectic bond-density-wave is naturally caused by the paramagnon interference mechanism, because strong scatterings among different van-Hove singularity points are induced. In addition, the fluctuations of the bond-order induce sizable “beyond-Migdal” pairing glue, and therefore both singlet nodal  $s$ -wave pairing and triplet  $p$ -wave pairing states are expected to emerge. The coexistence of both states would explain exotic superconducting states. Unexpected similarities between kagome metal and some Fe-based superconductors are discussed. This study enables us to understand the exotic density wave, superconductivity and their interplay in kagome metals based on the interference mechanism.

Rich quantum phase transitions in strongly correlated metals with multiple degrees of freedom and geometrical frustration were discovered one after another recently [1–4]. To understand such rich phase transitions, a significant ingredient is various quantum interference processes between different fluctuations [5–12]. The recent discovery of unconventional density-wave (DW) order and exotic superconductivity in kagome lattice metal  $AV_3Sb_5$  ( $A=K, Rb, Cs$ ) have triggered enormous amount of researches [13–20]. The prominent interplay between density-wave and superconductivity in addition to geometrical frustration have attracted considerable attention in kagome metals with strong correlation. This discovery sparked lots of theoretical studies [21–27].

At ambient pressure,  $AV_3Sb_5$  exhibits charge-channel DW order at  $T_{DW} = 78, 94$  and  $102$  K for  $A=K, Cs$  and  $Rb$ , respectively [13, 14, 28, 29]. Below  $T_{DW}$ ,  $2 \times 2$  (inverse) star of David pattern is observed by STM studies [30, 31]. The absence of acoustic phonon anomaly at  $T_{DW}$  [32] would exclude strong electron-phonon coupling driven DW state. As possible electron-correlation-driven DW orders, charge/bond orders and loop current orders [22, 24–27, 33–35] have been proposed theoretically, mainly based on the extended Hubbard model with the on-site ( $U$ ) and the nearest-site ( $V$ ) Coulomb interactions. However, when  $V \ll U$  due to Thomas-Fermi screening, previous studies predicted the strong spin-density-wave (SDW) instability, in contrast to the tiny SDW instability in  $AV_3Sb_5$  at  $T_{DW}$  [28, 29, 36].

Below  $T_{DW}$ , exotic nodal superconductivity occurs at  $T_c = 1 \sim 3$  K at ambient pressure. [18, 19]. The Hebel-Slichter peak in  $1/T_1T$  [29] and small impurity effect on  $T_c$  [37] indicate the singlet  $s$ -wave superconducting (SC) state. On the other hand, possibilities of triplet pairing state [38] and nematic SC state [39, 40] have been reported, which indicates non- $s$  wave pairing states. In addition, possibility of topological states has been discussed intensively [41]. Under pressure,  $T_{DW}$  decreases

and vanishes at the DW quantum critical point (DW-QCP) at  $P \sim 2$  GPa. For  $A=Cs$ ,  $T_c$  exhibits nontrivial double SC dome in the DW phase, and the highest  $T_c$  ( $\lesssim 10$  K) is realized at the DW-QCP [15]. In addition, theoretical phonon-mediated  $s$ -wave  $T_c$  is too low to explain experiments [23]. Thus, unconventional SC state due to DW fluctuations [42, 43] is naturally expected in  $AV_3Sb_5$ .

The current central issues would be summarized as: (i) Origin of the DW state and its driving mechanism, (ii) SC state and its mechanism, and (iii) Interplay between DW and superconductivity. To attack these issues, it is useful to focus on the similarity to Fe-based superconductors, in which  $s$ -wave state appears next to the nematic and smectic orbital/bond orders. These orders are naturally explained in terms of the quantum interference mechanism: The interference among optical phonons [5], and/or spin fluctuations [6, 9, 10, 44] (at wavevectors  $\mathbf{q}$  and  $\mathbf{q}'$ ) give rise to unconventional DW at  $\mathbf{q} + \mathbf{q}'$ , which is shown in Fig. 1 (a). This mechanism is also applicable to various nematic/smectic orders in transition metal compounds [45–48] and  $f$ -electron systems [49]. It is meaningful to investigate the interplay between interference mechanism, van Hove singularity (vHS) points and sublattice degrees of freedom in kagome metal. Its lattice and band structure and Fermi surface (FS) are shown in Figs. 1 (b), (c) and (d), respectively.

In this paper, we study the unconventional DW order in  $AV_3Sb_5$  due to beyond-mean-field effects, and its interplay with exotic SC states. By optimizing the form factor that represents the nonlocal ( $=\mathbf{k}$ -dependent) particle-hole (p-h) condensation, we derive the smectic bond-order at wavevector  $\mathbf{q}_n$  ( $n = 1, 2, 3$ ) even when spin fluctuations are tiny. Its driving force is the paramagnon interference, which provides large “nonlocal” backward and umklapp scattering among different vHS points. In addition, the smectic DW fluctuations induce sizable “beyond-Migdal” pairing interaction. For this reason,

both nodal  $s$ -wave pairing and  $p$ -wave pairing states are expected to emerge. The coexistence of both states would explain exotic SC states in  $T$ - $P$  phase diagram [15, 16].

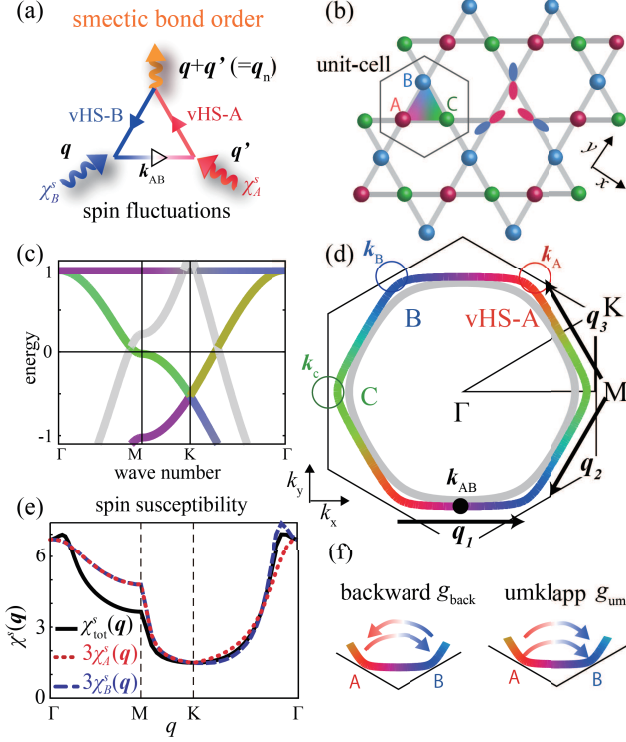


FIG. 1: (a) Smectic order at wavevector  $\mathbf{q}_n = \mathbf{q} + \mathbf{q}'$  driven by the paramagnon interference mechanism. (b) Kagome lattice structure of the vanadium-plane. Three  $b_{3g}$ -orbitals  $A, B, C$  (and three  $b_{2g}$ -orbitals  $A', B', C'$ ) are located at  $A, B, C$  sites, respectively. (c) Band structure and (d) FSs at  $n = 3.8$ . The outer (inner) FS are composed of  $b_{3g}$ - ( $b_{2g}$ -) orbitals. Three vHS points  $\mathbf{k}_A, \mathbf{k}_B$  and  $\mathbf{k}_C$  are respectively composed of  $A$  (red),  $B$  (blue), and  $C$  (green) orbitals. The inter-vHS nesting vectors  $\mathbf{q}_n$  ( $n = 1, 2, 3$ ) are shown. All  $b_{2g}$ -orbitals are expressed as gray color. (e)  $\chi_A^s(\mathbf{q})$ ,  $\chi_B^s(\mathbf{q})$ , and  $\chi_{\text{tot}}^s(\mathbf{q})$  in the RPA. (f) Backward and umklapp scattering among different vHS points. These processes are caused by paramagnon interference mechanism. (See Fig. 3 for detail.)

We analyze the following six orbital kagome lattice Hubbard model introduced in Ref. [24]. It is composed of three  $b_{3g}$ -orbitals ( $A, B, C$ ) and three  $b_{2g}$ -orbitals ( $A', B', C'$ ). Orbitals  $A$  and  $A'$  are located at  $A$  site, for instance. The kinetic term in  $\mathbf{k}$ -space is given as

$$H_0 = \sum_{\mathbf{k}, l, m, \sigma} \epsilon_{lm}(\mathbf{k}) c_{\mathbf{k}, l, \sigma}^\dagger c_{\mathbf{k}, m, \sigma}, \quad (1)$$

where  $l, m = A, B, C, A', B', C'$ . Hereafter the unit of energy is eV. The nearest-neighbor hopping integrals are  $t_{b3g} = 0.5$ ,  $t_{b2g} = 1$  and  $t_{b3g, b2g} = 0.002$ , and the on-site energies are  $E_{b3g} = -0.055$  and  $E_{b2g} = 2.17$  [24]. In the numerical study, it is convenient to analyze the six-orbital triangular lattice model in Fig. S1 in the Supplemental

Materials (SM) A [50], which is completely equivalent to the kagome metal in Fig. 1 (b). In the  $b_{3g}$ -orbital band shown in Fig. 1 (d), each vHS point ( $A, B$  and  $C$ ) is composed of pure orbital ( $A, B$  and  $C$ ), while the point  $\mathbf{k}_{AB} = (\mathbf{k}_A + \mathbf{k}_B)/2$  is composed of orbitals  $A$  and  $B$ . The present  $b_{3g}$ -orbital FS in the vicinity of three vHS points, on which the pseudogap opens below  $T_{\text{DW}}$  [51–54], well captures the observed FS [30, 55, 56].

Next, we introduce the “on-site Coulomb interaction” term  $H_U$ . It is composed of the intra- (inter-) orbital interaction  $U$  ( $U'$ ), and the exchange interaction  $J = (U - U')/2$ . Below, we fix the ratio  $J/U = 0.1$ . The  $4 \times 4$  matrix expression of on-site Coulomb interaction at each site,  $\hat{U}^{s(c)}$  for spin (charge) channel, is explained in the SM A [50]. In the mean-field-level approximation, the spin instability is the most prominent because of the largest interaction  $U$ . Figure 1 (e) exhibits the intra- $b_{3g}$ -orbital static ( $\omega = 0$ ) spin susceptibilities  $\chi_A^s(\mathbf{q}) \equiv \chi_{AA, AA}^s(\mathbf{q})$  and  $\chi_{\text{tot}}^s(\mathbf{q}) = \sum_m^{A, B, C} \chi_m^s(\mathbf{q})$  in the random phase approximation (RPA) at  $U = 1.26$  ( $\alpha_S = 0.80$  at  $T = 0.02$ ). In the RPA,  $\hat{\chi}^s(\mathbf{q}) = \hat{\chi}^0(\mathbf{q})(\hat{1} - \hat{\Gamma}^s \hat{\chi}^0(\mathbf{q}))^{-1}$ , where  $\hat{\chi}^0(\mathbf{q})$  is the irreducible susceptibility matrix and  $\mathbf{q} \equiv (\mathbf{q}, \omega_l = 2\pi T l)$ . The spin Stoner factor  $\alpha_S$  is the maximum eigenvalue of  $\hat{\Gamma}^s \hat{\chi}^0(\mathbf{q})$ , and SDW appears when  $\alpha_S = 1$ . Thus, intra-orbital spin susceptibility develops at  $\mathbf{q} \approx \mathbf{0}$  in the present kagome model. (Note that inter-orbital components, such as  $\chi_{AA, BB}^s$ , are small in magnitude because orbitals  $A$  and  $B$  correspond to different sites. Also,  $\chi_{A'}^s \ll \chi_A^s$ .)

Nonmagnetic DW orders cannot be explained in the RPA unless large nearest-neighbor Coulomb interaction  $V$  ( $V > 0.5U$ ) exists. However, beyond-RPA nonlocal correlations, called the vertex corrections (VCs), can induce various DW orders even for  $V = 0$  [5, 6, 9, 10, 44]. To consider the VCs due to the paramagnon interference in Fig. 1 (a), which causes the nematicity in Fe-based and cuprate superconductors, we employ the linearized DW equation [9, 46]:

$$\lambda_{\mathbf{q}} f_{\mathbf{q}}^L(k) = -\frac{T}{N} \sum_{p, M_1, M_2} I_{\mathbf{q}}^{L, M_1}(k, p) \times \{G(p)G(p + \mathbf{q})\}^{M_1, M_2} f_{\mathbf{q}}^{M_2}(p), \quad (2)$$

where  $I_{\mathbf{q}}^{L, M}(k, p)$  is the “electron-hole pairing interaction”,  $k \equiv (\mathbf{k}, \epsilon_n)$  and  $p \equiv (\mathbf{p}, \epsilon_m)$  ( $\epsilon_n, \epsilon_m$  are fermion Matsubara frequencies).  $L \equiv (l, l')$  and  $M_i$  represents the pair of  $d$ -orbital indices  $A, B, C, A', B', C'$ .  $\lambda_{\mathbf{q}}$  is the eigenvalue that represents the instability of the DW at wavevector  $\mathbf{q}$ , and  $\max_{\mathbf{q}} \{\lambda_{\mathbf{q}}\}$  reaches unity at  $T = T_{\text{DW}}$ .  $f_{\mathbf{q}}^L(k)$  is the Hermite form factor that is proportional to the p-h condensation  $\langle c_{\mathbf{k}+\mathbf{q}, l, \sigma}^\dagger c_{\mathbf{k}, l', \sigma} \rangle$ , or equivalently, the symmetry breaking component in the self-energy.

It is important to use appropriate kernel function  $I_{\mathbf{q}}^{L, M}$ , which is given as  $\delta^2 \Phi_{\text{LW}} / \delta G_{l'l}(k) \delta G_{mm'}(p)$  at  $\mathbf{q} = \mathbf{0}$  in the conserving approximation scheme [44, 57, 58],

where  $\Phi_{\text{LW}}$  is the Luttinger-Ward function. If we apply the bare interaction to  $I_{\mathbf{q}}^{L,M}$  that corresponds to RPA [58], the relation  $\lambda_{\mathbf{q}} > \alpha_S$  cannot be realized when  $H_U$  is local. Thus, higher-order corrections are indispensable.

Here, we apply the one-loop approximation for  $\Phi_{\text{LW}}$  [6, 44]. Then,  $I_{\mathbf{q}}^{L,M}$  is composed of one single-magnon exchange Maki-Thompson (MT) term and two double-magnon interference AL terms. Their diagrammatic expression (Fig. S2) and analytic one are explained in the SM B [50]. Due to the AL terms, nonmagnetic nematic order in FeSe is naturally reproduced even if spin fluctuations are very weak [6]. The importance of AL terms was verified by the functional-renormalization-group (fRG) study with constrained-RPA, in which higher-order parquet VCs are produced in an unbiased way, for several Hubbard models [4, 7, 45]. Later, we see that the AL diagrams induce the backward and umklapp scattering shown in Fig. 1 (f), and they mediate the p-h condensation at the inter-vHS nesting vector  $\mathbf{q}_1 = \mathbf{k}_B - \mathbf{k}_A$ .

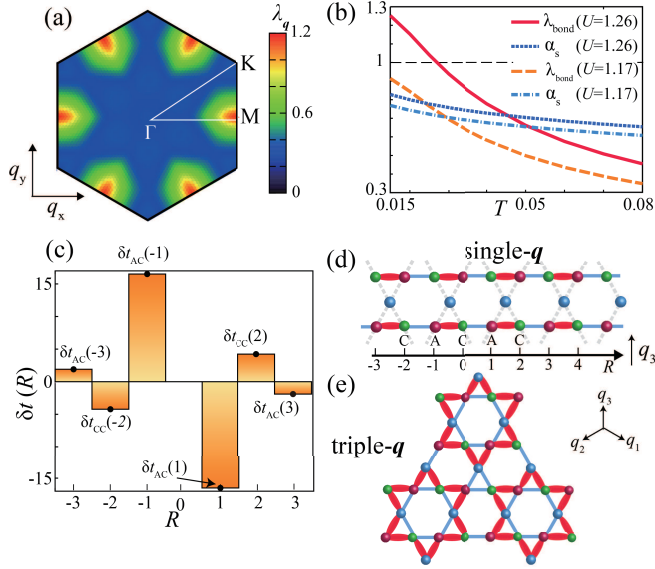


FIG. 2: (a) Obtained  $\mathbf{q}$ -dependence of the eigenvalue  $\lambda_{\mathbf{q}}$  at  $n = 3.8$  ( $T = 0.02$  and  $\alpha_S = 0.80$ ).  $\lambda_{\mathbf{q}}$  shows peaks at  $\mathbf{q}_n$  ( $n = 1, 2, 3$ ) shown in Fig. 1 (b), consistently with experiments in  $\text{AV}_3\text{Sb}_5$ . (b)  $T$ -dependences of  $\lambda_{\text{bond}}$  and  $\alpha_S$  at  $U = 1.26$  and  $1.17$ . The DW susceptibility ( $\chi_f^c(\mathbf{q}_n) \propto 1/(1 - \lambda_{\text{bond}})$ ) increases as  $T \rightarrow T_{\text{DW}} \approx 0.025$ , whereas magnetic susceptibility ( $\chi^s(\mathbf{0}) \propto 1/(1 - \alpha_S)$ ) is almost constant. (c) Obtained smectic bond-order, which corresponds to the modulation of hopping integrals. Its schematic picture at wavevector  $\mathbf{q}_3$  is shown in (d). (e) Expected triple- $\mathbf{q}$  star of David bond-order.

Figure 2 (a) exhibits the obtained  $\mathbf{q}$ -dependence of the eigenvalue  $\lambda_{\mathbf{q}}$  at  $n = 3.8$  ( $T = 0.02$  and  $\alpha_S = 0.80$ ). The obtained peak position at  $\mathbf{q}_n$  ( $n = 1, 2, 3$ ) is consistent with experiments in  $\text{AV}_3\text{Sb}_5$ . The  $T$ -dependences of  $\lambda_{\text{bond}} \equiv \lambda_{\mathbf{q}_n}$  and  $\alpha_S$  are shown in Fig. 2 (b). The DW susceptibility ( $\chi_f^c(\mathbf{q}_n) \propto 1/(1 - \lambda_{\text{bond}})$ ) increases as  $T \rightarrow T_{\text{DW}} \approx 0.025$ , whereas magnetic susceptibility

( $\chi^s(\mathbf{0}) \propto 1/(1 - \alpha_S)$ ) is almost constant.

Then, what order parameter is obtained? To answer this question, we perform the Fourier transform of the form factor:

$$\delta t_{lm}(\mathbf{r}) = \frac{1}{N} \sum_{\mathbf{k}} f_{\mathbf{q}_n}^{lm}(\mathbf{k}) e^{i\mathbf{r} \cdot \mathbf{k}}. \quad (3)$$

Then,  $\delta t_{lm}(\mathbf{r}_i - \mathbf{r}_j) \cos(\mathbf{q}_n \cdot \mathbf{r}_i + \theta)$  represents the modulation of the hopping integral between  $\mathbf{r}_i$  and  $\mathbf{r}_j$ , where  $\mathbf{r}_i$  represents the center of a unit-cell  $i$  in real space, and  $\theta$  is a phase factor. (The bond-order is  $\delta t_{lm}(\mathbf{r}) = \delta t_{ml}(-\mathbf{r})$  is real, and the current order is  $\delta t_{lm}(\mathbf{r}) = -\delta t_{ml}(-\mathbf{r})$  is imaginary.) Figure 2 (c) represents the obtained  $\delta t_{lm}(\mathbf{r})$  for  $\mathbf{q} = \mathbf{q}_3$  along the A-C direction. Here,  $(lm) = (CC)$  [(AC)] for  $\mathbf{r} = R\mathbf{a}_{\text{AC}}$  with even [odd] number  $R$ .

To summarize, we obtain the single- $\mathbf{q}$  smectic bond-order depicted in Fig. 2 (d). In SM C [50], we perform the DW equation analysis for  $n = 3.6$  and  $3.7$ , and obtain very similar results to Fig. 2. Thus, the robustness of the bond order is confirmed, irrespective of the Lifshitz transition at  $n \approx 3.71$ . In the triple- $\mathbf{q}$  state, in which three bond-orders with  $\mathbf{q}_1, \mathbf{q}_2, \mathbf{q}_3$  coexist, a star of David bond-order in Fig. 2 (e) appears. Figure S4 in SM D [50] shows the “unfolded” FS [59] under the triple- $\mathbf{q}$  order below  $T_{\text{DW}}$ . One can predict the emergence of the single- $\mathbf{q}$  or the triple- $\mathbf{q}$  state by analyzing the Ginzburg-Landau free energy up to the fourth-order terms [48].

We stress that the bond-order originates from the non-local VC in the kernel function  $I$  in Eq. (2). (Within the RPA,  $I (= -U)$  is a local function.) The dominant form factor at wavevector  $\mathbf{q} = \mathbf{q}_1$ ,  $f_{\mathbf{q}_1}^{lm}(\mathbf{k})$ , is given by  $(lm) = (AB)$  and  $(BA)$ . To understand its origin, we examine the kernel function at the lowest Matsubara frequency, multiplied with the  $b_{3g}$ -orbital weight ( $A, B$ , or  $C$ ) on two conduction bands at four outer points,  $\tilde{I}$ . Results are shown in Fig. 3: (a)  $\tilde{I}_{\mathbf{q}_1}^{AB,AB}(\mathbf{k}, \mathbf{k}_B)$  and (b)  $\tilde{I}_{\mathbf{q}_1}^{BA,AB}(\mathbf{k}, \mathbf{k}_B)$ , at  $T = 0.02$  and  $\alpha_S = 0.80$ . They are obtained in the triangular lattice model in Fig. S1 that is equivalent to the kagome metal. We see the strong developments of  $g_{\text{back}} \equiv \tilde{I}_{\mathbf{q}_1}^{AB,AB}(\mathbf{k}_B, \mathbf{k}_B)$  and  $g_{\text{um}} \equiv \tilde{I}_{\mathbf{q}_1}^{BA,AB}(\mathbf{k}_A, \mathbf{k}_B)$  expressed in Fig. 1 (e). (We note the relation  $\mathbf{k}_A + \mathbf{q}_1 = \mathbf{k}_B$ , and four outer momenta of  $I$  are defined in Fig. S2 (a).) Both scatterings contribute to the bond-order formation, as we clearly explain based on a simple two vHS model in SM C [50]. Microscopic origin of large  $g_{\text{back}}$  [ $g_{\text{um}}$ ] is the AL-VC with p-h [particle-particle (p-p)] pair shown in Fig. 3 (c) [(d)], because of the relation  $\chi_A^s, \chi_B^s \gg |\chi_{AA,BB}^s|$ . They are included as AL1 and AL2 in the kernel function  $I$ ; see SM B [50].

In Fig. 3 (e), we display the increment of  $\lambda_{\text{bond}}$ ,  $g_{\text{back}}$  and  $g_{\text{um}}$  with  $\alpha_S \propto U$  at  $T = 0.02$ . (The relation  $\lambda_{\text{bond}} \propto g_{\text{back}} + g_{\text{um}}$  holds, as we explain in SM C [50].) When  $\alpha_S = 0.75$ , then  $\lambda_{\text{bond}} \approx 0.88$ ,  $g_{\text{um}} \approx 2$  and  $g_{\text{back}} \approx 1$ , respectively. Thus, both  $g_{\text{um}}$  and  $g_{\text{back}}$  are comparable or larger than  $U$  due to the quantum interference mechanism in Fig. 1 (a). In the interference



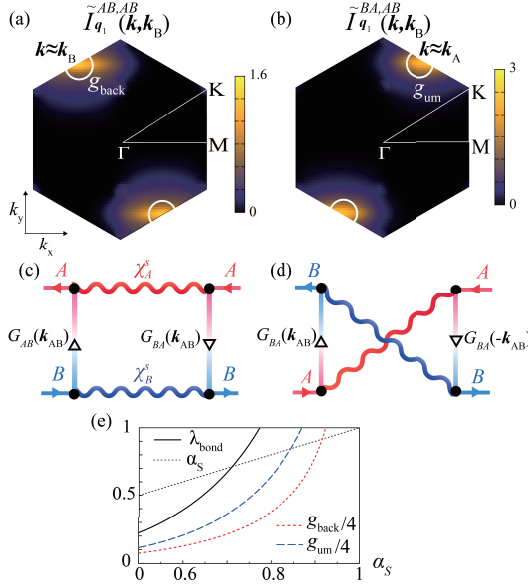


FIG. 3: Kernel function in the DW equation with orbital weights at the lowest Matsubara frequency: (a)  $\tilde{I}_{q_1}^{AB,AB}(\mathbf{k}, \mathbf{k}_B)$  and (b)  $\tilde{I}_{q_1}^{BA,AB}(\mathbf{k}, \mathbf{k}_B)$  for  $\alpha_S = 0.80$ . Four outer momenta of kernel function are defined in Fig. S2 (a) in SM B [50]. The former at  $\mathbf{k} = \mathbf{k}_B$  and the latter at  $\mathbf{k} = \mathbf{k}_A$  give  $g_{\text{back}}$  and  $g_{\text{um}}$ , respectively. Both scatterings contribute to the bond-order formation. (c) AL-VC with p-h pair and (d) that with p-p pair. The former (latter) gives large  $g_{\text{back}}$  ( $g_{\text{um}}$ ). (e)  $\lambda_{\text{bond}}$ ,  $g_{\text{back}}$  and  $g_{\text{um}}$  as functions of  $\alpha_S$  at  $T = 0.02$ .

mechanism in Figs. 3 (c) and (d), the inter-orbital Green function  $G_{AB}(\mathbf{k})$  is significant. As understood from Fig. 1 (b),  $G_{AB}(\mathbf{k})$  is large at  $\mathbf{k} \sim \mathbf{k}_{AB}$ , while it vanishes at  $\mathbf{k} = \mathbf{k}_A$  and  $\mathbf{k}_B$ . Therefore, the FS portion away from vHS points is indispensable in deriving the smectic order.

Finally, we study the unconventional superconductivity mediated by bond-order fluctuations. Here, we solve the following linearized SC gap equation on the FSs:

$$\lambda^{\text{SC}} \Delta_{\mathbf{k}}(\epsilon_n) = \frac{\pi T}{(2\pi)^2} \sum_{\epsilon_m} \oint_{\text{FSs}} \frac{d\mathbf{k}'}{v_{\mathbf{k}'}} \frac{\Delta_{\mathbf{k}'}(\epsilon_m)}{|\epsilon_m|} V_{s(t)}^{\text{SC}}(\mathbf{k}, \mathbf{k}'), \quad (4)$$

where  $\Delta_{\mathbf{k}}(\epsilon_n)$  is the gap function on FSs, and  $v_{\mathbf{k}}$  is Fermi velocity. The eigenvalue  $\lambda^{\text{SC}}$  reaches unity at  $T = T_c$ . The diagrammatic expression of Eq. (4) is given in Fig. 4 (a).  $V_{s(t)}^{\text{SC}}$  is the singlet/triplet pairing interaction in the band-basis, due to the triple- $\mathbf{q}$  bond-order fluctuations ( $V_{\text{bond}}$ ) and spin fluctuations ( $\propto \chi^s$ ) derived in SM E [50]. The former term for  $\mathbf{k}' - \mathbf{k} \approx \mathbf{q}_1$  is

$$\frac{1}{2} \frac{\bar{f}_{\mathbf{q}}(\mathbf{k}) \bar{f}_{\mathbf{q}_1}(\mathbf{k}) \bar{f}_{\mathbf{q}_1}(-\mathbf{k}')^*}{1 - \lambda_{\text{bond}}} \frac{1}{1 + \xi^2(\mathbf{q}_1 - (\mathbf{k}' - \mathbf{k}))^2}, \quad (5)$$

where  $\bar{f}_{\mathbf{q}}(\mathbf{k})$  is the Hermite form factor in the band-basis, and  $\bar{f}_{\text{bond}} = g_{\text{um}}$  if we set  $|\bar{f}_{\mathbf{q}_1}(\mathbf{k}_A)| = 1$ . Both  $\lambda_{\text{bond}}$  and  $g_{\text{um}}$  are already obtained in Fig. 3 (e), and the numerator of Eq. (5) on outer FS is given in Fig. S6 in SM E [50].

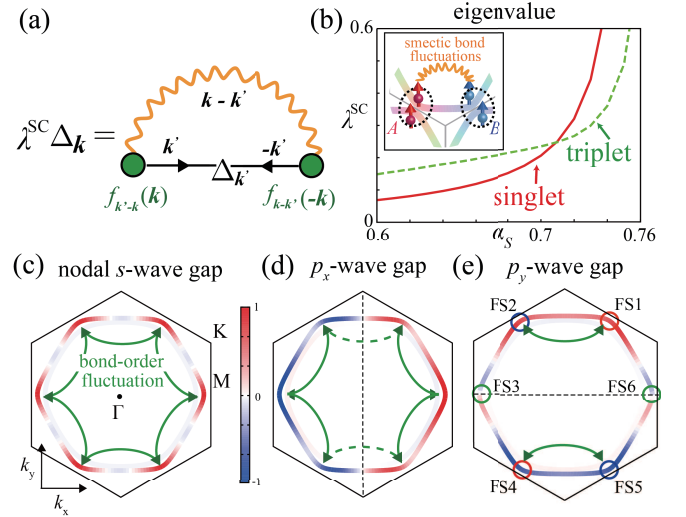


FIG. 4: (a) Pairing gap equation due to bond-order fluctuations. The form factor  $f$  gives the nonlocal (beyond-Migdal) electron-boson coupling function. (b) Obtained eigenvalues of gap equation for the singlet  $s$ -wave ( $A_{1g}$ ) and the triplet  $p$ -wave ( $E_{1u}$ ) states. Obtained gap functions for (c)  $s$ -wave state and (d)(e)  $p$ -wave state are shown. Green full (broken) arrow lines represent the smectic fluctuations between vHS points with the same (opposite) sign gap functions.

Figure 4 (b) shows the obtained  $\lambda^{\text{SC}}$  at  $T = 0.02$  and  $\xi = 1.0$ , where  $p$ -wave triplet ( $s$ -wave singlet) state is expected to appear when  $\alpha_S \lesssim 0.7$  ( $\gtrsim 0.7$ ). Figure 4 (c) shows the nodal  $s$ -wave gap function on  $b_{3g}$ -orbital FS for  $\alpha_S = 0.75$ , and  $p_x, p_y$ -wave ones for  $\alpha_S = 0.70$  are shown in Figs. 4 (d) and (e). Note that obtained SC gap on inner FS made of  $b_{2g}$ -orbital is very small, while it can be large due to (for instance) finite inter-band electron-phonon interaction.

Here, we discuss the origin of  $s/p$ -wave SC state. Triple- $\mathbf{q}$  bond-order fluctuations work as attraction between FS*i* and FS(*i* + 1), where FS*i* (*i* = 1 ~ 6) is the FS portion around vHS points shown in Fig. 4 (e). Therefore, six pairs shown by green full arrows contribute to the  $s$ -wave state in Fig. 4 (c). In contrast, only two pairs contribute to the  $p_y$ -wave state in Fig. 4 (e). (In the  $p_x$ -wave state in Fig. 4 (d), four pairs (two pairs) give positive (negative) contribution.) Therefore, the  $s$ -wave state is obtained for  $\alpha_S \gtrsim 0.7$ , where  $\lambda_{\text{bond}}$  exceeds  $\alpha_S$ . In Fig. 4 (c), we show the obtained nodal  $s$ -wave gap due to the repulsive interaction by spin fluctuations, while nodes will be lifted by impurity scattering. In contrast, the  $p$ -wave state is obtained for  $\alpha_S \lesssim 0.7$ , because weak ferro-spin-fluctuations favor (destroy) the triplet (singlet) pairing. Thus, the present bond-order + spin fluctuation mechanism predicts rich  $s$ - and  $p$ -wave SC states.

In summary, we derived the smectic bond-order in  $\text{AV}_3\text{Sb}_5$  due to the paramagnon interference mechanism, irrespective of tiny magnetic criticality in kagome metal

because of the prominent vHS and geometrical frustration. In addition, we predicted that the emergence of nodal  $s$ -wave and  $p$ -wave SC states owing to the cooperation of bond-order and SDW fluctuations. This mechanism may explain high- $T_c$  state in  $\text{CsV}_3\text{Sb}_5$  under pressure. The present study would give crucial hints to understand recently discovered “smectic order and adjacent high- $T_c$  state” in  $\text{FeSe}/\text{SrTiO}_3$  [60]. It is noteworthy that the paramagnon interference mechanism also responsible for loop current orders, which are the condensations of “odd-parity”  $p$ -h pairs [61, 62]. It is important to study the current order mechanism in kagome metals in future because the emergence of current orders has been hotly discussed experimentally [30, 63, 64].

This study has been supported by Grants-in-Aid for Scientific Research from MEXT of Japan (JP18H01175, JP17K05543, JP20K03858, JP20K22328), and by the Quantum Liquid Crystal No. JP19H05825 KAKENHI on Innovative Areas from JSPS of Japan.

- 
- [1] E. Fradkin and S. A. Kivelson, *Nat. Phys.* **8**, 864 (2012).
  - [2] J. C. Davis and D.-H. Lee, *Proc. Natl. Acad. Sci. USA* **110**, 17623 (2013).
  - [3] T. Shibauchi, T. Hanaguri, and Y. Matsuda, *J. Phys. Soc. Jpn.* **89**, 102002 (2020).
  - [4] R. Tazai, Y. Yamakawa, M. Tsuchiizu, and H. Kontani, *arXiv:2105.01872*.
  - [5] H. Kontani, T. Saito, and S. Onari, *Phys. Rev. B* **84**, 024528 (2011).
  - [6] S. Onari and H. Kontani, *Phys. Rev. Lett.* **109**, 137001 (2012).
  - [7] M. Tsuchiizu, Y. Ohno, S. Onari and H. Kontani *Phys. Rev. Lett.* **111**, 057003 (2013).
  - [8] Y. Yamakawa and H. Kontani, *Phys. Rev. Lett.* **114**, 257001 (2015).
  - [9] S. Onari, Y. Yamakawa, and H. Kontani, *Phys. Rev. Lett.* **116**, 227001 (2016).
  - [10] Y. Yamakawa, S. Onari, and H. Kontani, *Phys. Rev. X* **6**, 021032 (2016).
  - [11] A. V. Chubukov, M. Khodas, and R. M. Fernandes, *Rhys. Rev. X* **6**, 041045 (2016).
  - [12] R. M. Fernandes, P. P. Orth, and J. Schmalian, *Annual Review of Condensed Matter Physics* **10**, 133 (2019)
  - [13] B. R. Ortiz, L. C. Gomes, J. R. Morey, M. Winiarski, M. Bordelon, J. S. Mangum, I. W. H. Oswald, J. A. Rodriguez-Rivera, J. R. Neilson, S. D. Wilson, E. Ertekin, T. M. McQueen, and E. S. Toberer, *Phys. Rev. Materials* **3**, 094407 (2019).
  - [14] B. R. Ortiz, S. M. L. Teicher, Y. Hu, J. L. Zuo, P. M. Sarte, E. C. Schueller, A. M. M. Abeykoon, M. J. Krogstad, S. Rosenkranz, R. Osborn, R. Seshadri, L. Balents, J. He, and S. D. Wilson, *Phys. Rev. Lett.* **125**, 247002 (2020).
  - [15] F. H. Yu, D. H. Ma, W. Z. Zhuo, S. Q. Liu, X. K. Wen, B. Lei, J. J. Ying, and X. H. Chen, *Nat Commun* **12**, 3645 (2021).
  - [16] K. Y. Chen, N. N. Wang, Q. W. Yin, Z. J. Tu, C. S. Gong, J. P. Sun, H. C. Lei, Y. Uwatoko, and J.-G. Cheng, *Phys. Rev. Lett.* **126**, 247001 (2021).
  - [17] B. R. Ortiz, P. M. Sarte, E. M. Kenney, M. J. Graf, S. M. L. Teicher, R. Seshadri, and S. D. Wilson, *Phys. Rev. Materials* **5**, 034801 (2021).
  - [18] Q. Yin, Z. Tu, C. Gong, Y. Fu, S. Yan, and H. Lei, *Chinese Phys. Lett.* **38**, 037403 (2021).
  - [19] C. C. Zhao, L. S. Wang, W. Xia, Q. W. Yin, J. M. Ni, Y. Y. Huang, C. P. Tu, Z. C. Tao, Z. J. Tu, C. S. Gong, H. C. Lei, Y. F. Guo, X. F. Yang, and S. Y. Li, *arXiv:2102.08356*.
  - [20] W. Duan, Z. Nie, S. Luo, F. Yu, B. R. Ortiz, L. Yin, H. Su, F. Du, A. Wang, Y. Chen, X. Lu, J. Ying, S. D. Wilson, X. Chen, Y. Song, and H. Yuan, *arXiv:2103.11796*.
  - [21] R. Lou, A. Fedorov, Q. Yin, A. Kuibarov, Z. Tu, C. Gong, E. F. Schwier, B. Büchner, H. Lei, and S. Borisenko, *arXiv:2106.06497*.
  - [22] T. Park, M. Ye, and L. Balents, *arXiv:2104.08425*.
  - [23] H. Tan, Y. Liu, Z. Wang, and B. Yan, *arXiv:2103.06325*.
  - [24] X. Wu, T. Schwemmer, T. Muller, A. Consiglio, G. Sangiovanni, D. Di Sante, Y. Iqbal, W. Hanke, A. P. Schnyder, M. M. Denner, M. H. Fischer, T. Neupert, and R. Thomale, *arXiv:2104.05671*.
  - [25] X. Feng, K. Jiang, Z. Wang, and J. Hu, *arXiv:2103.07097*.
  - [26] C. Setty, H. Hu, L. Chen, and Q. Si, *arXiv:2105.15204*. Electron correlations and  $T$ -breaking density wave order in a  $\mathbb{Z}_2$  kagome metal
  - [27] Y.-P. Lin and R. M. Nandkishore, *arXiv:2104.02725*.
  - [28] D. W. Song, L. X. Zheng, F. H. Yu, J. Li, L. P. Nie, M. Shan, D. Zhao, S. J. Li, B. L. Kang, Z. M. Wu, Y. B. Zhou, K. L. Sun, K. Liu, X. G. Luo, Z. Y. Wang, J. J. Ying, X. G. Wan, T. Wu, and X. H. Chen, *arXiv:2104.09173*.
  - [29] C. Mu, Q. Yin, Z. Tu, C. Gong, H. Lei, Z. Li, and J. Luo, *Chin. Phys. Lett.* **38**, 077402 (2021).
  - [30] Y.-X. Jiang, J.-X. Yin, M. M. Denner, N. Shumiya, B. R. Ortiz, G. Xu, Z. Guguchia, J. He, M. S. Hossain, X. Liu, J. Ruff, L. Kautzsch, S. S. Zhang, G. Chang, I. Belopolski, Q. Zhang, T. A. Cochran, D. Multer, M. Litskevich, Z.-J. Cheng, X. P. Yang, Z. Wang, R. Thomale, T. Neupert, S. D. Wilson, and M. Z. Hasan, *arXiv:2012.15709*.
  - [31] H. Li, H. Zhao, B. R. Ortiz, T. Park, M. Ye, L. Balents, Z. Wang, S. D. Wilson, and I. Zeljkovic, *arXiv:2104.08209*.
  - [32] H. X. Li, T. T. Zhang, Y.-Y. Pai, C. Marvinney, A. Said, T. Yilmaz, Q. Yin, C. Gong, Z. Tu, E. Vescovo, R. G. Moore, S. Murakami, H. C. Lei, H. N. Lee, B. Lawrie, and H. Miao, *arXiv:2103.09769*.
  - [33] M. L. Kiesel, C. Platt, and R. Thomale, *Phys. Rev. Lett.* **110**, 126405 (2013).
  - [34] W.-S. Wang, Z.-Z. Li, Y.-Y. Xiang, and Q.-H. Wang, *Phys. Rev. B* **87**, 115135 (2013).
  - [35] J. Wen, A. Ruegg, C.-C. J. Wang, and G. A. Fiete, *Phys. Rev. B* **82**, 075125 (2010).
  - [36] E. M. Kenney, B. R. Ortiz, C. Wang, S. D. Wilson, and M. J. Graf, *J. Phys.: Condens. Matter* **33**, 235801 (2021).
  - [37] H.-S. Xu, Y.-J. Yan, R. Yin, W. Xia, S. Fang, Z. Chen, Y. Li, W. Yang, Y. Guo, and D.-L. Feng, *arXiv:2104.08810*.
  - [38] Y. Wang, S. Yang, P. K. Sivakumar, B. R. Ortiz, S. M. L. Teicher, H. Wu, A. K. Srivastava, C. Garg, D. Liu, S. S. P. Parkin, E. S. Toberer, T. McQueen, S. D. Wilson, and M. N. Ali, *arXiv:2012.05898*.
  - [39] S. Ni, S. Ma, Y. Zhang, J. Yuan, H. Yang, Z. Lu, N. Wang, J. Sun, Z. Zhao, D. Li, S. Liu, H. Zhang, H. Chen, K. Jin, J. Cheng, L. Yu, F. Zhou, X. Dong, J. Hu, H.-J. Gao, and Z. Zhao, *Chinese Phys. Lett.* **38**, 057403 (2021).

- [40] Y. Xiang, Q. Li, Y. Li, W. Xie, H. Yang, Z. Wang, Y. Yao, and H.-H. Wen, arXiv:2104.06909.
- [41] Z. Liang, X. Hou, W. Ma, F. Zhang, P. Wu, Z. Zhang, F. Yu, J.-J. Ying, K. Jiang, L. Shan, Z. Wang, and X.-H. Chen, arXiv:2103.04760.
- [42] R. Tazai and H. Kontani, Phys. Rev. B **98**, 205107 (2018).
- [43] R. Tazai and H. Kontani, J. Phys. Soc. Jpn **88**, 063701 (2019).
- [44] S. Onari and H. Kontani, Phys. Rev. Research **2**, 042005(R) (2020); S. Onari and H. Kontani, Phys. Rev. B **100**, 020507(R) (2019).
- [45] M. Tsuchiizu, K. Kawaguchi, Y. Yamakawa, and H. Kontani, Phys. Rev. B **97**, 165131 (2018).
- [46] K. Kawaguchi, Y. Yamakawa, M. Tsuchiizu, and H. Kontani, J. Phys. Soc. Jpn. **86**, 063707 (2017).
- [47] R. Tazai, Y. Yamakawa, M. Tsuchiizu, and H. Kontani, Phys. Rev. Research **3**, L022014 (2021).
- [48] T. Hirata, Y. Yamakawa, S. Onari, and H. Kontani, arXiv:2011.11272.
- [49] R. Tazai and H. Kontani, Phys. Rev. B **100**, 241103(R) (2019).
- [50] Supplemental Materials.
- [51] K. Nakayama, Y. Li, M. Liu, Z. Wang, T. Takahashi, Y. Yao, and T. Sato, arXiv:2104.08042.
- [52] Z. Liu, N. Zhao, Q. Yin, C. Gong, Z. Tu, M. Li, W. Song, Z. Liu, D. Shen, Y. Huang, K. Liu, H. Lei, and S. Wang, arXiv:2104.01125.
- [53] Z. Wang, S. Ma, Y. Zhang, H. Yang, Z. Zhao, Y. Ou, Y. Zhu, S. Ni, Z. Lu, H. Chen, K. Jiang, L. Yu, Y. Zhang, X. Dong, J. Hu, H.-J. Gao, and Z. Zhao, arXiv:2104.05556.
- [54] Z. Liu, N. Zhao, Q. Yin, C. Gong, Z. Tu, M. Li, W. Song, Z. Liu, D. Shen, Y. Huang, K. Liu, H. Lei, and S. Wang, rXiv:2104.01125.
- [55] Y. Hu, X. Wu, B. R. Ortiz, S. Ju, X. Han, J. Z. Ma, N. C. Plumb, M. Radovic, R. Thomale, S. D. Wilson, A. P. Schnyder, and M. Shi, arXiv:2106.05922.
- [56] Y. Luo, S. Peng, S. M. L. Teicher, L. Huai, Y. Hu, B. R. Ortiz, Z. Wei, J. Shen, Z. Ou, B. Wang, Y. Miao, M. Guo, M. Shi, S. D. Wilson, and J.-F. He, arXiv:2106.01248.
- [57] J. M. Luttinger and J. C. Ward, Phys. Rev. **118**, 1417 (1960).
- [58] G. Baym and L. P. Kadanoff, Phys. Rev. **124**, 287 (1961); G. Baym, Phys. Rev. **127**, 1391 (1962).
- [59] W. Ku, T. Berlijn, and C.-C. Lee, Phys. Rev. Lett. **104**, 216401 (2010).
- [60] Y. Yuan, X. Fan, X. Wang, K. He, Y. Zhang, Q.-K. Xue, and W. Li, Nat. Commun. **12**, 2196 (2021).
- [61] H. Kontani, Y. Yamakawa, R. Tazai, and S. Onari, Phys. Rev. Research **3**, 013127 (2021).
- [62] R. Tazai, Y. Yamakawa, and H. Kontani, Phys. Rev. B **103**, 161112 (2021).
- [63] S.-Y. Yang, Y. Wang, B. R. Ortiz, D. Liu, J. Gayles, E. Derunova, R. Gonzalez-Hernandez, L. Smejkal, Y. Chen, S. S. P. Parkin, S. D. Wilson, E. S. Toberer, T. McQueen, and M. N. Ali, Science Advances **6**, eabb6003 (2020).
- [64] F. H. Yu, T. Wu, Z. Y. Wang, B. Lei, W. Z. Zhuo, J. J. Ying, and X. H. Chen, arXiv:2102.10987.

[Supplementary Material]

# Mechanism of exotic density-wave and beyond-Migdal unconventional superconductivity in kagome metal $\text{AV}_3\text{Sb}_5$

Rina Tazai, Youichi Yamakawa, Seichiro Onari, and Hiroshi Kontani

*Department of Physics, Nagoya University, Nagoya 464-8602, Japan*

## A: Model Hamiltonian and RPA

In the main text, we analyze the kagome lattice model shown in Fig. 1 (b) introduced in Ref. [1]. In this model, a unit cell contains three sites (A, B, C), and each site possesses two orbitals ( $b_{3g}$  and  $b_{2g}$ ). In the theoretical analysis, it is more convenient to study a completely equivalent “six-orbital triangular lattice model” in Fig. S1: It is derived from the kagome lattice model by shifting three apical sites (A, B, C) of each upper triangular to its center, without changing the hopping integrals and the Coulomb interaction terms. One of the great merits of analyzing this triangular model is that any inter-site vector  $\mathbf{r}_i - \mathbf{r}_j$  is equal to a translation vector, and therefore functions in the momentum space (such as  $\chi_{ll',mm'}^s(\mathbf{q})$  and  $f_{\mathbf{q}}^{lm}(\mathbf{k})$ ) become periodic in the first Brillouin zone (BZ). For this reason, we perform the numerical study in the main text based on the triangular lattice model in Fig. S1.

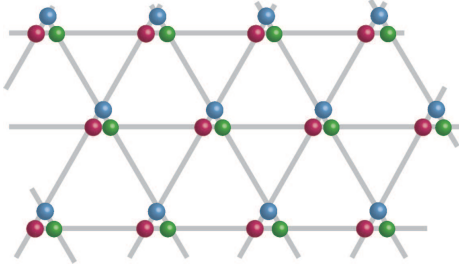


FIG. S1: **Six-orbital triangular lattice model:** In this model, three apical sites (A, B, C) of each upper triangular site in the kagome lattice are located at the same position. This model is convenient for the numerical study because both intra- and inter-orbital susceptibilities become periodic in the first BZ.

Next, we explain the multiorbital Coulomb interaction. The matrix expression of the spin-channel Coulomb interaction is [2–4]

$$U_{l_1 l_2, l_3 l_4}^s = \begin{cases} U, & l_1 = l_2 = l_3 = l_4 \\ U', & l_1 = l_3 \neq l_2 = l_4 \\ J, & l_1 = l_2 \neq l_3 = l_4 \\ J', & l_1 = l_4 \neq l_2 = l_3 \end{cases} \quad (\text{S1})$$

in the case that  $l_1 \sim l_4$  are orbitals ( $X, X'$ ) at site  $X$  ( $=A, B, C$ ). In other cases,  $U_{l_1 l_2, l_3 l_4}^s = 0$ . Also, the matrix

expression of the charge-channel Coulomb interaction is [2–4]

$$U_{l_1 l_2, l_3 l_4}^c = \begin{cases} -U, & l_1 = l_2 = l_3 = l_4 \\ U' - 2J, & l_1 = l_3 \neq l_2 = l_4 \\ -2U' + J, & l_1 = l_2 \neq l_3 = l_4 \\ -J', & l_1 = l_4 \neq l_2 = l_3 \end{cases} \quad (\text{S2})$$

in the case that  $l_1 \sim l_4$  are orbitals ( $X, X'$ ) at site  $X$  ( $=A, B, C$ ). In other cases,  $U_{l_1 l_2, l_3 l_4}^c = 0$ . Here,  $U$  ( $U'$ ) is the intra-orbital (inter-orbital) Coulomb interaction,  $J$  is the Hund’s coupling, and  $J'$  is the pair hopping term. In the main text, we assume the relations  $U = U' + 2J$  and  $J = J'$ , and set the constraint  $J/U = 0.10$ . The obtained results are not sensitive to the ratio  $J/U$ .

The spin (charge) susceptibility in the RPA,  $\chi_{ll',mm'}^{s(c)}(\mathbf{q})$ , is given as [2–4]

$$\hat{\chi}^{s(c)}(\mathbf{q}) = \hat{\chi}^0(\mathbf{q})(\hat{1} - \hat{U}^{s(c)}\hat{\chi}^0(\mathbf{q}))^{-1}, \quad (\text{S3})$$

where the element of the irreducible susceptibility is  $\chi_{ll',mm'}^0(\mathbf{q}) = -\frac{T}{N} \sum_{\mathbf{k}} G_{lm}(\mathbf{k} + \mathbf{q}) G_{m'l'}(\mathbf{k})$ .  $G_{lm}(\mathbf{k})$  is the  $(l, m)$  element of the electron Green function:  $\hat{G} = (\epsilon_n \hat{1} - \hat{H}_0(\mathbf{k}))^{-1}$ .

In the present model,  $\chi_{ll',mm'}^s(\mathbf{q})$  is very small unless all orbitals belong to  $b_{3g}$ . Also,  $\chi_{ll',mm'}^s(\mathbf{q})$  becomes large only when  $l = l' = m = m'$  and  $l = A$  or  $B$  or  $C$ . The spin susceptibility in the present model is shown in Fig. 1 (e) in the main text.

## B: Derivation of density-wave equation

Here, we derive the kernel function in the DW equation,  $I_{\mathbf{q}}^{ll',mm'}(k, k')$ , studied in the main text. It is given as  $\delta^2 \Phi_{\text{LW}} / \delta G_{l'l'}(k) \delta G_{mm'}(p)$  at  $\mathbf{q} = \mathbf{0}$  in the conserving approximation scheme [3, 5, 6], where  $\Phi_{\text{LW}}$  is the Luttinger-Ward function. Here, we apply the one-loop approximation for  $\Phi_{\text{LW}}$  [3, 4]. Then,  $I_{\mathbf{q}}^{L,M}$  in this kagome model is given as

$$I_{\mathbf{q}}^{ll',mm'}(k, k') = \sum_{b=s,c} \frac{a^b}{2} \left[ -V_{lm,l'm'}^b(k - k') + \frac{T}{N} \sum_p \sum_{l_1 l_2, m_1 m_2} V_{l_1 m_1}^b(p + \mathbf{q}) V_{m' m_2, l' l_2}^b(p) \right]$$



$$\begin{aligned}
& \times G_{l_1 l_2}(k-p)G_{m_2 m_1}(k'-p) \\
& + \frac{T}{N} \sum_p \sum_{l_1 l_2, m_1 m_2} V_{ll_1, m_2 m'}^b(p+\mathbf{q}) V_{m_1 m, l' l_2}^b(p) \\
& \times G_{l_1 l_2}(k-p)G_{m_2 m_1}(k'+p+\mathbf{q}) \Big] \quad (S4)
\end{aligned}$$

where  $a^{s(c)} = 3(1)$  and  $p = (\mathbf{p}, \omega_l)$ .  $\hat{V}^b$  is the  $b$ -channel interaction given by  $\hat{V}^b = \hat{U}^b + \hat{U}^b \hat{\chi}^b \hat{U}^b$ .  $\hat{U}^b$  is the matrix expression of the bare multiorbital Coulomb interaction for channel  $b$ .

The first term of Eq. (S4) corresponds to the single-magnon exchange Maki-Thompson (MT) term, and the second and third terms give two double-magnon interference Aslamazov-Larkin (AL) terms. They are expressed in Fig. S2 (a).

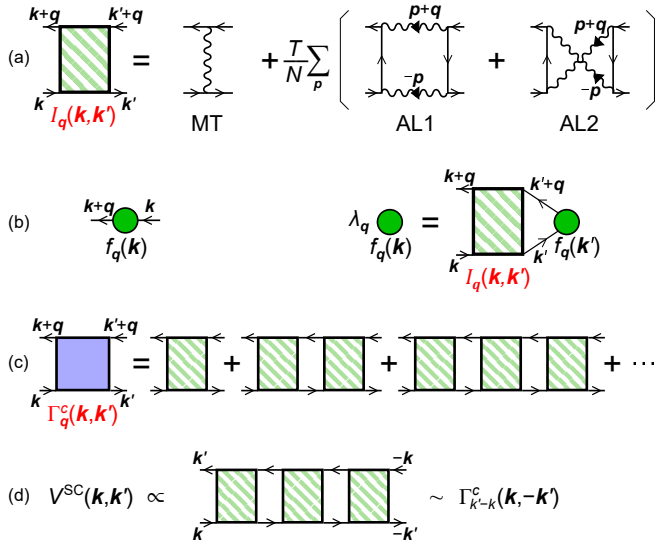


FIG. S2: **Derivations of DW equation and beyond-Migdal pairing interaction:** (a) Charge-channel kernel function  $I_q^{ll', mm'}(k, k')$  (b) Linearized DW equation. (c) Charge-channel full four-point vertex  $\Gamma_q^c(k, k')$  obtained by solving the DW equation. (d) Pairing interaction due to  $\Gamma_q^c$ :  $V^{SC}(k, k') \propto \Gamma_{k'-k}^c(k, -k')$ .

The density-wave (DW) instability driven by nonlocal beyond-mean-field correlation  $\hat{I}_q(k, k')$  is obtained by solving the DW equation introduced in Refs. [2, 3, 7]:

$$\begin{aligned}
\lambda_q f_q^{ll'}(k) &= \frac{T}{N} \sum_{k', m, m'} K_q^{ll', mm'}(k, k') f_q^{mm'}(k) \quad (S5) \\
K_q^{ll', mm'}(k, k') &= - \sum_{m'', m'''} I_q^{ll', m'', m'''}(k, k') \\
&\quad \times G_{m'' m}(k' + \mathbf{q}) G_{m' m'''}(k'), \quad (S6)
\end{aligned}$$

which is depicted in Fig. S2 (b). Here  $\lambda_q$  is the eigenvalue that reaches unity at the transition temperature.  $\hat{f}_q$  is the form factor of the DW order, which corresponds to the “symmetry-breaking in the self-energy”. By solving

Eq. (S5), we can obtain the optimized momentum and orbital dependences of  $\hat{f}$ . This mechanism has been successfully applied to explain the electronic nematic orders in Fe-based [2, 4, 8] and cuprate superconductors [9], and multipole orders in  $f$ -electron systems [10].

An arbitrary phase factor  $e^{i\alpha}$  can be multiplied to the solution of the linearized DW equation  $\hat{f}_q(k)$ . However, the phase factor should be determined uniquely so that  $\tilde{f}_q(\mathbf{k}) = (\hat{f}_q(\mathbf{k}, \pi T) + \hat{f}_q(\mathbf{k}, -\pi T))/2$  satisfies the Hermite condition  $\tilde{f}_q^{lm}(\mathbf{k}) = [\tilde{f}_{-q}^{ml}(\mathbf{k} + \mathbf{q})]^*$ .

Finally, we discuss the effective interaction driven by the bond-order fluctuations. By solving the DW equation (S5), we obtain the full four-point vertex function  $\Gamma_q^c(k, k')$  that is composed of  $I_q^c$  and  $G(k + \mathbf{q})G(k)$  shown in Fig. S2 (c), which increases in proportion to  $(1 - \lambda_q)^{-1}$ . Thus, we obtain the relation  $\Gamma_q^c(k, k') \approx f_q(k) \{f_q(k')\}^* \bar{I}_q^c (1 - \lambda_q)^{-1}$ , which is well satisfied when  $\lambda_q$  is a close to unity.

As we will discuss in SM E, the pairing interaction due to the bond-order fluctuations is given by the full four-point vertex:  $V^{SC}(\mathbf{k}, \mathbf{k}') \sim \Gamma_{\mathbf{k}' - \mathbf{k}}^c(\mathbf{k}, -\mathbf{k}') \sim f_{\mathbf{k}' - \mathbf{k}}(\mathbf{k}) \{f_{\mathbf{k}' - \mathbf{k}}(-\mathbf{k}')\}^* (1 - \lambda_q)^{-1}$ , which is depicted in Fig. S2 (d).

It is noteworthy that both the DW equation and the functional-renormalization group (fRG) method explain the nematic and smectic bond-order in single-orbital square lattice Hubbard models [7, 11] and anisotropic triangular lattice ones [12]. This fact means that higher-order diagrams other than MT or AL terms, that are included in the fRG method, are not essential in explaining the bond-order. Note that the contributions away from the conduction bands are included into  $N$ -patch fRG by applying the RG+cRPA method [9, 11, 12].

### C: Robustness of bond-order solution in the DW equation

In the main text, we present the numerical results for  $n = 3.8$ . In this case, the  $b_{3g}$ -orbital FS is very close to the vHS points on the BZ boundary as shown in Fig.1 (d), consistently with recent ARPES reports. In this model, the van Hove filling is  $n_{vHS} = 3.71$ , and the single large FS around  $\Gamma$  point is divided into two pockets around  $K$  and  $K'$  points for  $n < n_{vHS}$ . Thus, it is important to verify the robustness of numerical results for different electron filling  $n$ .

Figures S3 (a) and (b) represent the FS at  $n = 3.6$  and  $n = 3.7$ , respectively. The obtained eigenvalue of the DW equation at  $n = 3.6$  and  $n = 3.7$  in case of  $\alpha_S = 0.8$  is shown in Figs. S3 (c) and (d), respectively. Here,  $U = 1.34$  (1.25) for  $n = 3.6$  (3.7). In both cases, the smectic bond-order at  $\mathbf{q}_n$  ( $n = 1, 2, 3$ ) is satisfactorily obtained, irrespective of the Lifshitz transition at  $n_{vHS} = 3.71$ . Therefore, we conclude that the strong electron correlation due to the three vHS points is essential for



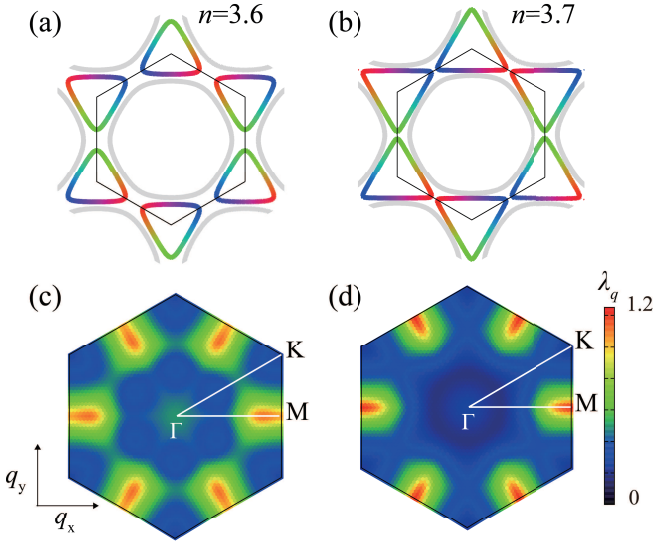


FIG. S3: **Robustness of bond-order solution:** (a) FS for  $n = 3.6$  and (b) FS for  $n = 3.7$ . (c)  $\mathbf{q}$ -dependence of the eigenvalue for  $n = 3.6$  and (d) that for  $n = 3.7$ .

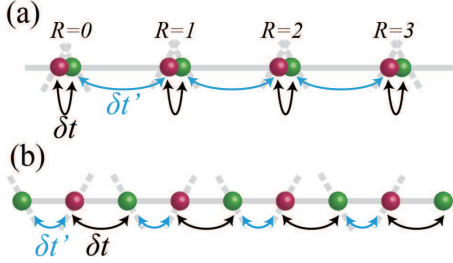


FIG. S4: **Origin of bond-order solution in kagome metal:** (a) Nearest-neighbor hopping modulations  $\delta t$  and  $\delta t'$  under the bond-order at  $\mathbf{q} = \mathbf{q}_3$  in the triangular lattice model in Fig. S1. (b)  $\delta t$  and  $\delta t'$  in the kagome lattice model in Fig. 1 (b).

the formation of the bond-order, while the shape and the topology of FS are not essential.

Based on this finding, we next discuss a simplified DW equation by focusing on the vHS points in order to understand why bond-order is obtained. For the bond-order at  $\mathbf{q} = \mathbf{q}_3$ , only vHS points A and C are essential, so we consider a simple two-component form factor  $(f_1, f_2) \equiv (f_{\mathbf{q}_3}^{CA}(\mathbf{k}_A), f_{\mathbf{q}_3}^{AC}(\mathbf{k}_C))$ . Then, the DW equation at  $\mathbf{q} = \mathbf{q}_3$  is given as

$$\lambda \begin{pmatrix} f_1 \\ f_2 \end{pmatrix} \sim N(0) \begin{pmatrix} g_{\text{back}} & g_{\text{um}} \\ g_{\text{um}} & g_{\text{back}} \end{pmatrix} \begin{pmatrix} f_1 \\ f_2 \end{pmatrix}, \quad (\text{S7})$$

where  $N(0)$  is the density-of-states at the Fermi level. As we explain in the main text, both  $g_{\text{back}}$  and  $g_{\text{um}}$  are positive. Thus, the largest eigenvalue and the eigenvector are  $\lambda \sim N(0)(g_{\text{back}} + g_{\text{um}})$  and  $\mathbf{f} = (1, 1)$ , respectively. After the Fourier transformation, the real-space form factor in the triangular lattice model in

Fig. S1 is given as  $\delta t_{CA}(R\mathbf{e}_\perp) \sim f_{CA}(\mathbf{k}_A)e^{i\pi R}$  and  $\delta t_{AC}(R\mathbf{e}_\perp) \sim f_{AC}(\mathbf{k}_C)e^{i\pi R}$ . Here,  $R$  is an integer, and  $\mathbf{e}_\perp$  is a unit vector perpendicular to  $\mathbf{q}_3$ . By making comparison between Fig. S1 and Fig. 1 (b), the nearest-neighbor hopping modulations in Fig. S4 (a) is given as  $(\delta t, \delta t') = (\delta t_{CA}(\mathbf{0}), \delta t_{AC}(\mathbf{e}_\perp)) \propto (1, -1)$ .

The same bond-order in the kagome lattice model is shown in Fig. S4 (b). When  $\delta t = -\delta t'$ , it is equivalent to Fig. 2 (d) in the main text. Therefore, the essential origin of the bond-order is naturally understood based on a simple two vHS model in Eq. (S7).

#### D: Unfolded Fermi surface under triple- $\mathbf{q}$ state

In the triple- $\mathbf{q}$  DW state, both the FS and the band-structure are folded into the folded BZ. They can be unfolded into the original size BZ [13], which correspond to the ARPES measurement in the DW state. The obtained unfolded FS in case of  $\max_{\mathbf{k}}\{f_{\mathbf{q}_n}(\mathbf{k})\} = 0.018$  eV is shown in Fig. S5. Here, the spectra around the vHS points are gapped. This result is consistent with the recent ARPES studies.

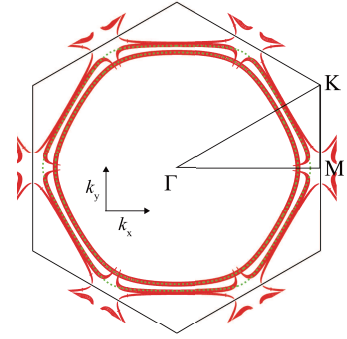


FIG. S5: **Unfolded FS under the triple- $\mathbf{q}$  bond-order:** The FS near the vHS points is reconstructed by the bond-order. The result for  $\max_{\mathbf{k}}\{f_{\mathbf{q}_n}(\mathbf{k})\} = 0.018$  eV is shown.

#### E: Derivation of SC gap equation

Here, we discuss the reason why bond-order fluctuations mediate the pairing interaction. In Ref. [14], the authors studied the orbital fluctuation mediated  $s$ -wave superconductivity in Fe-based superconductors. In that study, the electron-boson coupling (=form factor) is an orbital-dependent but  $\mathbf{k}$ -independent charge quadrupole operator:  $\hat{f}^{\mathbf{q}}(\mathbf{k}) = \hat{O}_\Gamma$  ( $\Gamma = xz, yz, xy$ ). In the main text, we obtain the development of bond-order fluctuations with the  $\mathbf{k}$ -dependent form factor in  $\text{AV}_3\text{Sb}_5$ , which is given by the nonlocal vertex corrections (VCs) that are dropped in the RPA. We reveal that bond-order fluctuations mediate significant “beyond-Migdal” pairing in-

interaction thanks to the  $\mathbf{k}$ -dependent form factor [3], and therefore  $s$ -wave and  $p$ -wave SC states emerge in  $\text{AV}_3\text{Sb}_5$ .

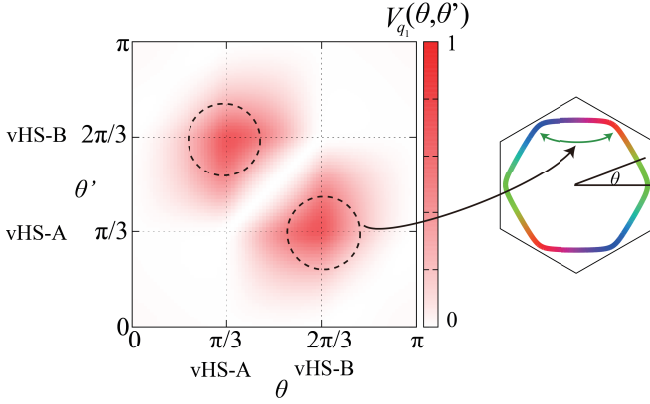


FIG. S6: **Pairing interaction on  $b_{3g}$ -orbital FS due to bond-order fluctuations:** We present  $V_1(\theta, \theta')$  due to  $\mathbf{q} \approx \mathbf{q}_1$  given in (S12) in case of  $\bar{I}_q = 1$  and  $\lambda_{\text{bond}} = 0$ . Here,  $\theta = \arctan(k_y/k_x)$  and  $\theta' = \arctan(k'_y/k'_x)$ .

In the following, we discuss the pairing interaction due to the bond-order fluctuations in kagome metal by following Ref. [3]. Hereafter, we drop the orbital indices just to simplify the notation. The pairing interaction between Cooper pairs  $(\mathbf{k}, -\mathbf{k})$  and  $(\mathbf{k}', -\mathbf{k}')$  due to charge-channel full four-point vertex in Fig. S2 (c) is given as  $V(\mathbf{k}, \mathbf{k}') \propto \Gamma_{\mathbf{k}'-\mathbf{k}}^c(\mathbf{k}, -\mathbf{k}')$ . We derive a convenient simple expression of  $\Gamma_{\mathbf{q}}^c(\mathbf{k}, \mathbf{k}')$ , we introduce the following approximation for the kernel function:

$$I_{\mathbf{q}}(\mathbf{k}, \mathbf{k}') = \bar{I}_{\mathbf{q}} f_{\mathbf{q}}(\mathbf{k}) f_{\mathbf{q}}^*(\mathbf{k}'), \quad (\text{S8})$$

where  $f_{\mathbf{q}}(\mathbf{k})$  is the form factor for the largest eigenvalue of the DW equation. By inserting Eq. (S8) into the DW equation, the eigenvalue is given as  $\lambda_{\mathbf{q}} = \bar{I}_{\mathbf{q}} \chi_f^0(\mathbf{q})$ , where

$$\chi_f^0(\mathbf{q}) = -\frac{T}{N} \sum_{\mathbf{k}} G(\mathbf{k} + \mathbf{q}) G(\mathbf{k}) \tilde{f}_{\mathbf{q}}(\mathbf{k}) \tilde{f}_{\mathbf{q}}^*(\mathbf{k}). \quad (> 0) \quad (\text{S9})$$

Then, the full four-point vertex is given as

$$\Gamma_{\mathbf{q}}^c(\mathbf{k}, \mathbf{k}') = \frac{\bar{I}_{\mathbf{q}} f_{\mathbf{q}}(\mathbf{k}) f_{\mathbf{q}}^*(\mathbf{k}')}{1 - \lambda_{\mathbf{q}}}. \quad (\text{S10})$$

Therefore, the pairing interaction is  $V(\mathbf{k}, \mathbf{k}') = \frac{\bar{I}_{\mathbf{q}} f_{\mathbf{q}}(\mathbf{k}) f_{\mathbf{q}}^*(-\mathbf{k}')}{1 - \lambda_{\mathbf{q}}}$ , where  $\mathbf{q} = \mathbf{k}' - \mathbf{k}$ . Note that the relation  $f_{\mathbf{q}}^*(-\mathbf{k}') = f_{-\mathbf{q}}(-\mathbf{k})$  holds for  $\mathbf{q} = \mathbf{k}' - \mathbf{k}$  due to the Hermite condition of the form factor.

Considering that the  $\mathbf{q}$ -dependence of the form factor is moderate, the total pairing interaction due to triple- $\mathbf{q}$  bond-order fluctuations is approximately given as

$$V_{\text{bond}}(\mathbf{k}, \mathbf{k}') = \frac{1}{2} \sum_n^{1,2,3} V_n(\mathbf{k}, \mathbf{k}'), \quad (\text{S11})$$

$$\begin{aligned} V_n(\mathbf{k}, \mathbf{k}') &= \frac{\bar{I}_{\mathbf{q}} \tilde{f}_{\mathbf{q}_n}(\mathbf{k}) \tilde{f}_{\mathbf{q}_n}^*(-\mathbf{k}')}{1 - \lambda_{\mathbf{k}'-\mathbf{k}}} \\ &\approx \frac{\bar{I}_{\text{bond}} \tilde{f}_{\mathbf{q}_n}(\mathbf{k}) \tilde{f}_{-\mathbf{q}_n}(-\mathbf{k}')}{1 - \lambda_{\text{bond}}} \frac{1}{1 + \xi^2(\mathbf{q}_n - (\mathbf{k}' - \mathbf{k}))^2}, \end{aligned} \quad (\text{S12})$$

where  $\tilde{f}^{\mathbf{q}}(\mathbf{k}) \equiv \sum_{l,m} \tilde{f}_{lm}^{\mathbf{q}}(\mathbf{k}) u_{l,b}(\mathbf{k} + \mathbf{q})^* u_{m,b}(\mathbf{k})$ . Here,  $u_{l,b}(\mathbf{k}) = \langle l, \mathbf{k} | b, \mathbf{k} \rangle$  is the unitary transformation matrix element between orbital  $l$  and conduction band  $b$ , and  $\tilde{f}^{\mathbf{q}}(\mathbf{k}) \equiv (f^{\mathbf{q}}(\mathbf{k}, \pi T) + f^{\mathbf{q}}(\mathbf{k}, -\pi T))/2$ . We also approximate  $\lambda_{\mathbf{q}} \approx \lambda_{\text{bond}} - b(\mathbf{q} - \mathbf{q}_n)^2$  with  $b \approx \xi^2(1 - \lambda_{\text{bond}})$  for  $\mathbf{q} \sim \mathbf{q}_n$ . Here, we set  $\tilde{f}_{\mathbf{q}_1}^{BA}(k_B) = 1$ . Then, the coupling constant  $\bar{I}_{\text{bond}}$  is directly given by  $g_{\text{um}}$  that is obtained in the main text. We stress that  $\tilde{f}_{\mathbf{q}_n}(\mathbf{k}) \tilde{f}_{-\mathbf{q}_n}(-\mathbf{k})$  is positive for even-parity bond-order.

Figure S6 is the pairing interaction  $V_1(\theta, \theta')$  on the  $b_{3g}$ -orbital FS due to the bond-order fluctuations at wavevector  $\mathbf{q} \approx \mathbf{q}_1$  by setting  $\bar{I}_{\mathbf{q}} = 1$ ,  $\lambda_{\text{bond}} = 0$  and  $\xi = 0$ . Here,  $\theta = \arctan(k_y/k_x)$  and  $\theta' = \arctan(k'_y/k'_x)$ . Thus, strong attractive pairing interaction is induced by the bond-order fluctuations around the vHS points. This is the driving force of the  $s$ -wave and  $p$ -wave pairing states obtained in the main text.

In the main text, we solve the gap equation in the presence of bond and spin fluctuations.

$$V_s^{\text{SC}}(\mathbf{k}, \mathbf{k}') = V_{\text{bond}}(\mathbf{k}, \mathbf{k}') - \frac{3}{2} U^2 \chi^s(\mathbf{k} - \mathbf{k}') - U, \quad (\text{S13})$$

$$V_t^{\text{SC}}(\mathbf{k}, \mathbf{k}') = V_{\text{bond}}(\mathbf{k}, \mathbf{k}') + \frac{1}{2} U^2 \chi^s(\mathbf{k} - \mathbf{k}'), \quad (\text{S14})$$

where  $s$  ( $t$ ) represents the singlet (triplet) pairing interaction. The diagrammatic expression of the gap equation due to  $V_{\text{bond}}(\mathbf{k}, \mathbf{k}')$  is depicted in Fig. 4 (a) in the main text. In solving the gap equation, we set the BCS cutoff energy  $\omega_c$  for  $V_{\text{bond}}$  because the energy-scale of bond-order fluctuations is much smaller than  $E_F$ . Here, we set  $\omega_c = 0.02$ . Note that the pairing interaction for the band  $b, b'$  can be derived from that in the orbital representation by using the unitary transformation matrix  $u_{l,b}(\mathbf{k})$ .

It is noteworthy that the present bond-order fluctuating pairing mechanism is outside of the Migdal approximation, in which the form factor is assumed to be  $\mathbf{k}$ -independent. The present bond-order fluctuating mechanism has close similarity to the multiple-fluctuation pairing mechanism developed in Refs. [3, 15, 16].

- 
- [1] X. Wu, T. Schwemmer, T. Muller, A. Consiglio, G. Sangiovanni, D. Di Sante, Y. Iqbal, W. Hanke, A. P. Schnyder, M. M. Denner, M. H. Fischer, T. Neupert, and R. Thomale, arXiv:2104.05671.
  - [2] S. Onari, Y. Yamakawa, and H. Kontani, Phys. Rev. Lett. **116**, 227001 (2016).

- [3] S. Onari and H. Kontani, Phys. Rev. Research **2**, 042005(R) (2020); S. Onari and H. Kontani, Phys. Rev. B **100**, 020507(R) (2019).
- [4] S. Onari and H. Kontani, Phys. Rev. Lett. **109**, 137001 (2012).
- [5] J. M. Luttinger and J. C. Ward, Phys. Rev. **118**, 1417 (1960).
- [6] G. Baym and L. P. Kadanoff, Phys. Rev. **124**, 287 (1961); G. Baym, Phys. Rev. **127**, 1391 (1962).
- [7] K. Kawaguchi, Y. Yamakawa, M. Tsuchiizu, and H. Kontani, J. Phys. Soc. Jpn. **86**, 063707 (2017).
- [8] Y. Yamakawa, S. Onari, and H. Kontani, Phys. Rev. X **6**, 021032 (2016).
- [9] R. Tazai, Y. Yamakawa, M. Tsuchiizu, and H. Kontani, arXiv:2105.01872.
- [10] R. Tazai and H. Kontani, Phys. Rev. B **100**, 241103(R) (2019).
- [11] M. Tsuchiizu, K. Kawaguchi, Y. Yamakawa, and H. Kontani, Phys. Rev. B **97**, 165131 (2018).
- [12] R. Tazai, Y. Yamakawa, M. Tsuchiizu, and H. Kontani, Phys. Rev. Research **3**, L022014 (2021).
- [13] W. Ku, T. Berlijn, and C.-C. Lee, Phys. Rev. Lett. **104**, 216401 (2010).
- [14] H. Kontani, T. Saito, and S. Onari, Phys. Rev. B **84**, 024528 (2011).
- [15] R. Tazai and H. Kontani, Phys. Rev. B **100**, 241103 (2019).
- [16] R. Tazai and H. Kontani, J. Phys. Soc. Jpn **88**, 063701 (2019).